

Remarkable polarization sensitivity of gold nanoparticle arrays

Brian K. Canfield,^{a)} Sami Kujala, and Martti Kauranen

Institute of Physics, Tampere University of Technology, P. O. Box 692 FI-33101 Tampere, Finland

Konstantins Jefimovs, Tuomas Vallius, and Jari Turunen

Department of Physics, University of Joensuu, P. O. Box 111 FI-80101 Joensuu, Finland

(Received 23 September 2004; accepted 22 March 2005; published online 28 April 2005)

In an array of low-symmetry, L-shaped gold nanoparticles, slight distortions of particle shape and arm lengths eliminate the array's mirror plane. Such asymmetries induce large angular shifts ($\sim 10^\circ$) of the resonant extinction axes directions from those of mirror-symmetric particles. The axes directions exhibit dispersion, as allowed by the lack of any structural features dictating them. The nanostructures are chiral, and evidence of optical activity is observed. Rigorous diffraction theory calculations qualitatively reproduce the data. © 2005 American Institute of Physics.

[DOI: 10.1063/1.1924886]

The linear and nonlinear optical properties of arrays of metal nanoparticles command considerable attention at present. Many recent studies have focused on determining the optical properties of particles possessing high degrees of symmetry, such as spheroids,¹ ellipsoids,² and rings.³ The extinction spectra of more complicated structures, such as cylindrical and trigonal prism arrays^{4,5} have also been reported. Studies on arrays of gammadion metal particles, which possess inherently chiral structure, have demonstrated optical activity for subwavelength particles in zeroth order,⁶ and for suprawavelength particles in higher diffracted orders.⁷ The ability to control precisely the fabrication of metal nanoparticle arrays has many application prospects, including spectrally encoded data storage.⁸

In this article we report on the sensitivity of arrays of low-symmetry, L-shaped metal nanoparticles to the polarization state of light. Previous studies of similar samples found that particle orientation within the array affects the linear and nonlinear responses,⁹ showing that the smallest details of the array structure have significant impact on its optical response. Our measurements on particles with minor shape deviations from ideal reinforce and expand upon this observation.

Subwavelength arrays of gold nanoparticles were fabricated with a Leica LION LV-1 electron beam lithography (EBL) tool and standard lift-off process.⁹ The beam energy during exposure was $E=15$ keV, the beam current was $I=90$ pA, and the step size was 5 nm. A completed nanoparticle cross section consists of a glass substrate, a 2 nm Cr adhesion layer (which does not extend beyond the particle perimeter), 20 nm of gold, and 20 nm of protective glass. The particles were written to have ~ 200 nm arm lengths, 110 nm linewidth, and 400 nm array period. The array covers $(600\text{ }\mu\text{m})^2$. The symmetry of an ideal "L" with equal arm lengths suggests a natural choice of principal axes, denoted X and Y (inset, Fig. 1). The ideal array then possesses a mirror plane along X , the only symmetry axis in the XY plane. (Since the experiments were performed at normal incidence, we neglect the Z axis.) The actual nanoparticles, however, acquire small shape distortions from ideal during fabrication.

Close scrutiny of the micrograph also reveals that the vertical arms are about 5% longer than the horizontal arms, likely due to a small astigmatism of the beam.

We acquired linear extinction spectra by measuring the referenced transmission T of X and Y input polarizations with a StellarNet, Inc. (Oldmar, Florida) fiber optic spectrometer (range 500–1200 nm) and white light source [extinction equals $\log(1/T)$]. Substrate-only transmission was used as the reference. The nanoparticle arrays are strongly dichroic, with a 200 nm separation between the main resonances. We focus on the longer-wavelength resonances because they were found to depend on particle size and spacing, whereas the peak near 670 nm appears independently of these quantities. The resonant Y peak is approximately twice as strong as the X peak (Fig. 1). Both wavelength and magnitude differences can be related to the shape of the particles.⁸ Studies of elliptical particles have demonstrated that varying their aspect ratio produces large peak separations between long- and short-axis polarizations, with long-axis polarization extinction greater than short-axis extinction.¹⁰

To study the polarization properties of the sample further, we measured transmittance as a function of the direction of linear input polarization θ . Two different wavelengths near the resonances were used: 820 nm (X) and 1060 nm (Y).

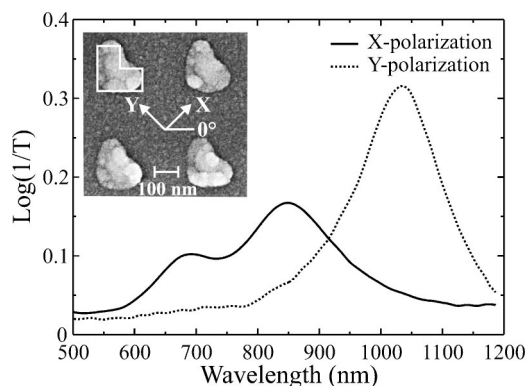


FIG. 1. X - and Y -polarized extinction spectra. Inset: scanning electron micrograph of the sample, ideal particle shape (dotted outline), and coordinate system. Sample alignment 45° from the EBL system is experimentally convenient.

^{a)} Author to whom correspondence should be addressed; electronic mail: brian.canfield@tut.fi

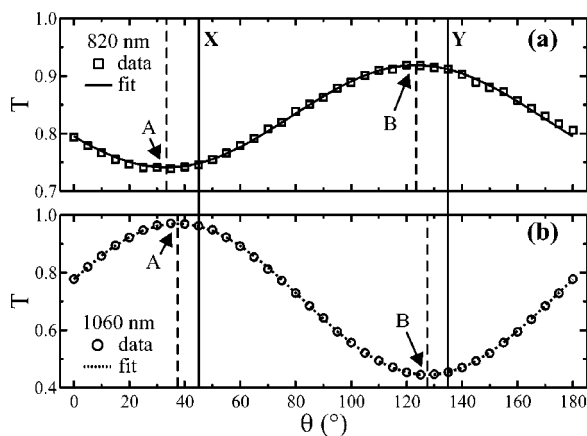


FIG. 2. Transmittances and fits to a transmission model at (a) 820 nm and (b) 1060 nm (uncertainty: ± 0.02). Vertical lines: solid, mirror-symmetry axes; dashed, measured axes.

Each microwatt-power beam was chopped, then polarized with a high-quality calcite polarizer. The incident polarization angle was controlled by rotating a Fresnel rhomb, which acts as a broadband half-wave plate. The beam was then moderately focused onto the sample array at normal incidence with a 20 cm focal length lens. A photodiode and lock-in amplifier referenced to the chopper frequency were used for detection. A reference scan through the substrate only was again measured.

We discover a large displacement of the primary axes from their expected locations at 45° (X) and 135° (Y) (Fig. 2). The locations of these primary axes, marked as A and B in Fig. 2, can be determined by fitting the data to a simple transmission model $T = T_A \cos^2(\theta - 45^\circ - \alpha) + T_B \sin^2(\theta - 45^\circ - \alpha)$, where T_A and T_B are the transmittances along the A and B axes, respectively, and α is the shift angle [45° relates the sample and EBL systems (Fig. 1)].

The fits in Fig. 2 describe the data exceptionally well. At 820 nm, the fitted shift angle is $\alpha = -11.5^\circ \pm 0.1^\circ$, while at 1060 nm, $\alpha = -7.6^\circ \pm 0.1^\circ$. Since the response of the samples is frequency-dependent, and the shape of the actual particles does not dictate the direction of the principal axes, wavelength dispersion of the axes is possible.¹¹ It is clear that ideal symmetry no longer holds, and this symmetry breaking should render the array chiral, which manifests as optical activity. To check for optical activity, we performed polarization azimuth rotation measurements and sought a nonzero average rotation. A second calcite polarizer (analyzer) was therefore inserted before the detector and the relative difference Δ between the incident polarization and output polarization azimuth angles was then recorded (Fig. 3).

We note that the overall magnitude of azimuth rotation is about three times greater at 1060 nm than at 820 nm, related to the extinction strength difference between the two wavelengths. We can predict the expected azimuth rotation for a given transmission curve, relying on the fact that if linearly polarized light is absorbed more strongly along one primary axis, the transmitted field will appear to have its polarization rotated relative to the incident light. Based on our earlier transmission model, the predicted rotation becomes $\Delta = \arctan[\sqrt{T_B/T_A} \tan(\theta - 45^\circ - \alpha)] - (\theta - 45^\circ - \alpha)$. Note that this model assigns all rotation to dichroism (real T_A and T_B), and hence neglects the effects of birefringence and optical activity. Any deviation of the measured results will thus indicate the presence of effects beyond dichroism.

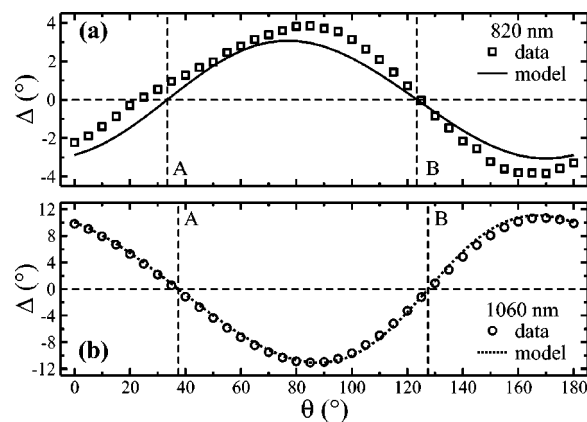


FIG. 3. Polarization azimuth rotation data and dichroism-based models at (a) 820 nm and (b) 1060 nm (uncertainty: $\pm 0.1^\circ$). Dashed lines: horizontal, zero-crossing guides; vertical, axes A and B.

dedicate the presence of effects beyond dichroism.

The predictions from this simple model match the data very well at 1060 nm [Fig. 3(b)]. The average rotation at this wavelength -0.04° is essentially zero given uncertainty. In addition, the zero crossings are separated by 90° and align with the A and B axes, so there is apparently no measurable optical activity at 1060 nm. At 820 nm, on the other hand, we find that the data deviates significantly from the model. Here the average rotation is $\approx 0.3^\circ$, well above uncertainty. Moreover, the zero crossings of this data are distinctly separated by 102° . Taken together, these observations support the presence of optical activity at 820 nm, which serves to emphasize broken symmetry and non-ideal nanoparticles.

We performed rigorous diffraction theory calculations using the Fourier modal method¹² to determine both the transmission and polarization azimuth rotation [Figs. 4(a) and 4(b), respectively] at 820 nm, based on geometrically ideal, asymmetric nanoparticles (190 nm \times 200 nm arms, 110 nm linewidth, 20 nm thick, with planar surfaces and right corners). Unfortunately, computations at 1060 nm are infeasible since gold's conductivity here requires too many additional Fourier coefficients for convergence.¹³ The transmission curve [Fig. 4(a)] displays a smaller shift angle in the same direction as the experimental data, while the shape of the rotation curve [Fig. 4(b)] closely resembles the data from

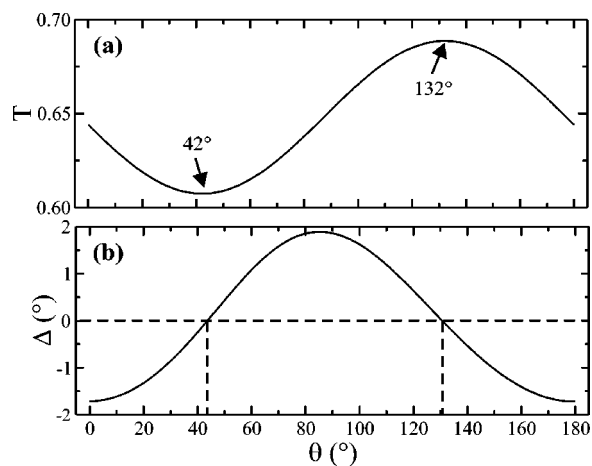


FIG. 4. Plots of rigorous diffraction theory calculations at 820 nm: (a) transmission spectrum and (b) polarization azimuth rotation (dashed lines: zero-crossing separation).

Fig. 3(a). The average azimuth rotation is a mere -0.004° , of opposite sign and two orders of magnitude smaller than the experimental result. The zero crossings, however, are separated by 87° , a nonorthogonal value in qualitative agreement with experiment. The calculations also show that the true eigenpolarizations of the sample are elliptical and, therefore, A and B are not the true principal axes of the sample.

The quantitative differences strongly imply that the small shape deviations of individual particles (such as rounded corners, protrusions, and uneven height profiles of Fig. 1) exert a large influence on their optical response. Random defects should average out over many particles, but a slight directional bias due to electron beam scanning and asymmetric arm lengths would survive and contribute to measured polarization effects. This indicates that the array structure may also play a role, but further investigation of this topic is necessary. We emphasize, however, that rigorous diffraction theory can qualitatively describe the observed optical responses. In addition, further investigations into the array's second-harmonic response reveal strong, symmetry-forbidden signals.¹⁴

In conclusion, arrays of low-symmetry metal nanoparticles can exhibit exceptional polarization sensitivity. Small structural deviations of L-shaped particles from ideal were shown to affect the optical response significantly. The principal directions of extinction were found to be rotated by $\sim 10^\circ$ from those of geometrically ideal, mirror-symmetric particles. The broken symmetry of the structures makes them chiral, and results show weak optical activity at the wavelength 820 nm. The high degree of polarization sensitivity of the arrays suggests that similar structures could find applica-

tions in polarization-dependent optical components. However, the extreme sensitivity of the optical response to the smallest details of the structure needs to be well-considered in any potential application.

The authors thank Yu. Svirko for productive discussions. Funding was from the Academy of Finland (102018, 101362).

- ¹W. Rechberger, A. Hohenau, A. Leitner, J. R. Krenn, B. Lamprecht, and F. R. Aussenegg, *Opt. Commun.* **220**, 137 (2003).
- ²K.-H. Su, Q.-H. Wei, X. Zhang, J. J. Mock, D. R. Smith, and S. Schultz, *Nano Lett.* **3**, 1087 (2003).
- ³J. Aizpurua, P. Hanarp, D. S. Sutherland, M. Käll, G. W. Bryant, and F. J. G. de Abajo, *Phys. Rev. Lett.* **90**, 057401 (2003).
- ⁴C. L. Haynes, A. D. McFarland, L. L. Zhao, R. P. V. Duyne, G. C. Schatz, L. Gunnarsson, J. Prikulis, B. Kasemo, and M. Käll, *J. Phys. Chem. B* **107**, 7337 (2003).
- ⁵K. L. Kelly, E. Coronado, L. L. Zhao, and G. C. Schatz, *J. Phys. Chem. B* **107**, 668 (2003).
- ⁶T. Vallius, K. Jefimovs, J. Turunen, P. Vahimaa, and Y. Svirko, *Appl. Phys. Lett.* **83**, 234 (2003).
- ⁷A. Papakostas, A. Potts, D. M. Bagnall, S. L. Prosvirnin, H. J. Coles, and N. I. Zheludev, *Phys. Rev. Lett.* **90**, 107404 (2003).
- ⁸H. Ditlbacher, J. R. Krenn, B. Lamprecht, A. Leitner, and F. R. Aussenegg, *Opt. Lett.* **25**, 563 (2000).
- ⁹H. Tuovinen, M. Kauranen, K. Jefimovs, P. Vahimaa, T. Vallius, and J. Turunen, *J. Nonlinear Opt. Phys. Mater.* **11**, 421 (2002).
- ¹⁰W. Gotschy, K. Vonmetz, A. Leitner, and F. R. Aussenegg, *Appl. Phys. B: Lasers Opt.* **63**, 381–384 (1996).
- ¹¹M. Born and E. Wolf, *Principles of Optics*, 7th ed. (Cambridge University, Cambridge, England, 1999).
- ¹²L. Li, *J. Opt. Soc. Am. A* **14**, 2758 (1997).
- ¹³L. Li, *J. Opt. A, Pure Appl. Opt.* **1**, 531 (1999).
- ¹⁴B. K. Canfield, S. Kujala, K. Jefimovs, J. Turunen, and M. Kauranen, *Opt. Express* **12**, 5418 (2004).